https://doi.org/10.71252/2177-34912025720006
ISSN: 2177-3491

Multispectral images in the monitoring of coffee trees phytotechnical parameters after pruning[1]

Renato Aurélio Severino de Menezes Freitas[2*], *Gleice Aparecida de Assis*[3], *George Deroco Martins*[4], *Renan Zampiroli*[5], *Letícia Gonçalves do Nascimento*[6], *Nathalia Oliveira de Araújo*[6]

ABSTRACT

The objective of this work was to monitor coffee plants (*Coffea arabica* L.) after pruning through multispectral images obtained with an unmanned aerial vehicle (UAV) containing a *Mapir Survey 3* camera and estimate agronomic parameters based on simple regression parametric models. Growth evaluation was performed in 228 sampling points related to the coffee plants. The parameters analyzed were plant height, crown diameter, plagiotropic branch length, and the number of plagiotropic branches after the pruning point. The creation of mosaics was performed through the software *Agisoft PhotoScan Professional 1.4.5*, and radiometric calibration through *Mapir Camera Control*, georeferenced by *QGIS* and normalized by *ENVI*. Based on the models generated, data analysis permitted estimating coffee plants' agronomic parameters after decote-type pruning (cutting off the orthotropic branch at 1.5 m and 2.0 m above ground) with high accuracy. Height was measured in April's flight with the near-infrared band (Precision = 91.87%), crown diameter and plagiotropic branches length in April's flight with the infrared band (Precision = 89.36% and 82.22%, respectively), number of nodes in February's flight with the near-infrared band (Precision = 79.48%), and the number of plagiotropic branches after the pruning point in June's flight with the near-infrared band (Precision = 69.57%).

Keywords: *Coffea arabica* L., NDVI, decote-type pruning, UAV, estimation.

[1] This article was extracted from the first author's Master Dissertation which is available at http://doi.org/10.14393/ufu.di.2020.846.

[2] Universidade Federal de Uberlândia, Programa de Pós-graduação em Agricultura e Informações Geoespaciais, Monte Carmelo, MG, Brazil. renato.freitas@ufu.br

[3] Universidade Federal de Uberlândia, Instituto de Ciências Agrárias (ICIAG), Monte Carmelo, MG, Brazil. gleice@ufu.br

[4] Universidade Federal de Uberlândia, Faculdade de Engenharia Civil (FECIV), Uberlândia, MG, Brazil. deroco@ufu.br

[5] Universidade Federal de Uberlândia, Programa de Pós-Graduação em Agronomia, Umuarama, MG, Brazil. renanzampiroli@ufu.br

[6] Universidade Federal de Uberlândia, Monte Carmelo, MG, Brazil. leticia.goncalves5220@gmail.com; natyaraujo2008@hotmail.com

*Corresponding author: renato.freitas@ufu.br

Editors:
Danielle Fabíola Pereira da Silva

Submitted: April 3rd, 2022.
Accepted: August 30th, 2024.

INTRODUCTION

The cultivation of coffee trees of the species *Coffea arabica* L. is characterized by being an activity conducted in large areas. As it is a perennial culture, alternative management tactics that will make it possible and sustainable will be required. Pruning is a recovery management of coffee plants, being a viable alternative and widely used in older, depleted crops and that will make the renovation in order to increase the longevity of the coffee trees, maintaining the productive stability and the final quality of the product (Assis *et al*., 2018).

As occurs in pruning management, technological advancements introduced in agricultural systems have raised producers' interest in adopting tools that can enhance monitoring and operational management. The use of vegetation remote sensing and unmanned aerial vehicle (UAV) for monitoring and multispectral images obtention aims to provide identification of the farm's spatial variation, cost reduction (spending resources according to the property's demands), data and information organization (to enhance costly traditional management tactics) (Santos *et al*., 2019).

Multispectral remote sensing is a high potential tool for monitoring and identifying spatial variability in coffee plantations using vegetation indices (Mahajan *et al*., 2014). Besides helping producers in operational management, it also provides accuracy in data acquisition and decision-making, reducing operational costs. Marin *et al*. (2019) demonstrated that vegetation monitoring through multispectral cameras attached to UAVs reduced operational costs, providing a more efficient and fast data collection regarding the plantation's evolutive stages, contributing to management tactics' decision-making.

Thus, this study is important due to the lack of research concerning evaluating the phytotechnical potential of coffee trees after pruning through multispectral images. In this sense, the producer might have an estimation tool for the plants' vegetative growth. It is possible to estimate the growth parameters through the most responsive spectral bands and determine which season or phenological stage is more appropriate for performing aerial surveys and data collection. Therefore, this study might provide a basis for future research related to the phytotechnical growth of coffee tree after pruning.

This research aims to monitor coffee plants of the species *C. arabica* L. after pruning through multispectral images obtained by a UAV and estimate agronomic parameters based on simple regression models.

MATERIAL AND METHODS

The experiment was conducted at the Federal University of Uberlândia, *Campus* Monte Carmelo, located at the state of Minas Gerais, in the mesoregion of Triângulo Mineiro and Alto Paranaíba. The experimental site geographical coordinates are 18º 43' 41" S, 47º 31'26" W, and 903 m of altitude. Planting occurred in December 2015 with 3.5 m between rows and 0.6 m between plants. The experimental site comprised eight coffee cultivars, arranged in a randomized block design (RBD) with 38 blocks. Each experimental unit was composed of one line with ten plants; the six central plants were considered useful (Figure 1).

Low decote-type pruning with a standard height of 1.5 m was conducted on September 13, 2019, using a chainsaw. The sampling points were obtained by receptors GNSS Promark 200 using a fast relative static positioning method. Afterward, post-processing was performed through the Brazilian network of GNSS system's continuous monitoring (RBMC).

The aerial surveys were planned in the software *DroneDeploy* with a GSD (Ground Sample Distance) of 3 cm, 100 m above the soil. The vehicle used was the *Drone Phantom 4 Advanced* with a camera *Mapir Survey 3*, operating in the electromagnetic spectrum regions red (B_{650nm}), green (B_{560nm}), and near-infrared (B_{980nm}). The flights were performed on 09/20/2019, 11/01/2019, 13/02/2020, 20/04/2020, 24/06/2020, and 01/09/2020 between 12h and 13h.

Growth evaluations were performed in 228 sampling points of the coffee plants and were considered useful six plants from each of the 38 blocks of the experiment. The evaluations were conducted on the same days of the flights, and the following characteristics were measured:

Plant height: obtained by measuring the height from the beginning of the stem to the terminal bud with a centimeter scale.

Crown diameter: measured with a centimeter scale using the two branches in the direction between the rows that presented the higher length as a mensuration pattern.

Number of nodes by plagiotropic shoot: obtained by counting the nodes in a plagiotropic shoot located at the middle third of the plant in both crown projection sites.

Length of plagiotropic branches: determined by measuring with a centimeter scale a plagiotropic shoot at the middle third of the plant from its insertion in the orthotropic shoot until the extremity of the plagiotropic shoot.

Number of plagiotropic branches: obtained by counting the productive nodes after a pruning point.

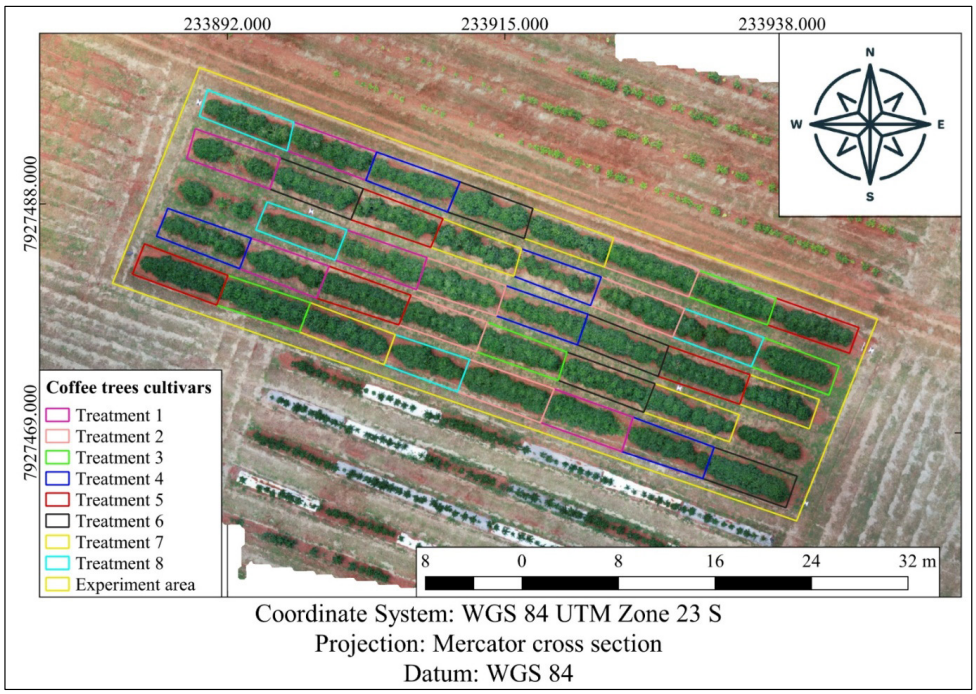

Figure 1: Layout of the experimental area and the respective boundaries of the plots and the coffee treatments, where: T1: Acaiá Cerrado MG-1474: early to medium ripening cycle and red fruits; T2: Mundo Novo IAC 379-19: medium ripening cycle and red fruits, T3: Bourbon Amarelo IAC J10: early ripening cycle and yellow fruits; T4: Catuaí Vermelho IAC 99: late ripening cycle and red fruits; T5: Topázio MG-1190: medium ripening cycle and yellow fruits; T6: Acauã Novo: medium to late ripening cycle and red fruits; T7: IAC 125 RN: early ripening cycle and red fruits; T8: Paraíso MG H 419-1: medium ripening cycle and yellow fruits. Adapted from Freitas et al. 2023.

After the image obtention, the software *Agisoft PhotoScan Professional 1.4.5* was used to generate the mosaics, consisting of the union of common scenes of many images in the same feature. Radiometric calibration of mosaics was performed through the software *Mapir Camera Control,* inserting the image of the calibration target of the *Mapir Survey 3*, then identifying the different spectral patterns of the image. Mosaics' georeferencing was performed with the software *QGIS 3.2* through the points collected in field research after post-processing through RBMC to enhance precision.

Because it is a temporal analysis, the mosaics were exported to the software ENVI to normalize the images. Through the tool *Region of interesting (ROI Tool)*, the mean values of the bands B_{650nm}, B_{560nm}, and B_{980nm} in the grayscale were extracted.

Afterward, correlation analysis was performed using the Pearson correlation coefficient between the bands B_{650nm}, B_{560nm}, and B_{980nm} of the normalized mosaics and the agronomic parameters presented. Within the bands with better correlation with the parameters, that is, P-value < 0.05, the ones that would compose the prediction models were chosen through simple regression, considered a parametric technique of continuous variables estimation.

The models were generated based on the regression between 183 samples, and 45 of them were excluded for the posterior validation of the regeneration models, forming a total of 228 sampling points. The models of simple parametric regression were chosen for the generation of the estimation models for agronomic parameters. Among the equations generated, those with better adaptation to the data were chosen. Thus, Root-Mean-Squared Error (RMSE) (equations 1 and 2) was used to determine the accuracy of the estimation models. For such a procedure, 45 samples among the 228 were randomly excluded and served as checkpoints for the regressions generation to determine the accuracy of the prediction models for agronomic parameters.

$$RMSE = \sqrt{\sum_{i=1}^{n} \frac{(Xo - Xe)^2}{n}} \quad (1)$$

$$RMSE(\%) = \sqrt{\sum_{i=1}^{n} \frac{(Xo - Xe)^2}{n}} \times \frac{100 \times n}{\sum_{i=1}^{n} Xe} \quad (2)$$

Where: RMSE is the Root-Mean-Squared Error; RMSE (%) is the Root-Mean-Squared Error percentage; *Xo* represents the values of the agronomic parameters observed *in situ*; *Xe* represents the values of estimated agronomic parameters; *n* is the number of samples.

The mosaics that presented a significant correlation between the bands and the agronomic parameters were exported to the software *ENVI.* The registration of the images in the software was performed considering six points in common between the images, based on an RMSE < 0,05.

The regression equations generated from the significant correlations between the bands and the agronomic parameters were exported to the software *ENVI*. Through the tool *BandMath*, thematic maps were generated based on the regressions that presented the lower RMSE. Those that better encompassed the data and estimated the variable with better precision.

Growth rates were developed by exporting the images to the software *ENVI* and selecting Equations 3 and 4 in the tool *Band math*. To obtain the growth rate by the number of months, the regression equation of the image with the higher development value was subtracted by the image with the lower value. The resultant value was divided by the number of months between the evaluations for the parameters analyzed.

$$Tx = \frac{(B1 - B2)}{n} \tag{3}$$

$$Tx = \left[\frac{(B1 - B2)}{n}\right] \times 100 \tag{4}$$

Where: *Tx* is the growth rate; *B1* is the regression equation of the image with higher development; *B2* is the regression equation of the image with lower development; *n* is the number of months between the evaluations; *100* is the conversion rate from *m* to *cm*.

After detecting indices that presented significant correlation according to the Pearson correlation coefficient, those with lower Root-Mean-Squared Error (RMSE) were selected. It means that the model that presented higher precision to estimate agronomic parameters after pruning was selected. The graphics and thematic maps were then generated for each agronomic parameter evaluated in 228 sampling points regarding the experimental site's useful plants.

RESULTS AND DISCUSSION

The correlation data obtained through the Pearson correlation coefficient shows that the flights of September and November 2019 did not present a significant correlation between the bands and the agronomic parameters (P-value > 0.05).

The February's flight presented significant correlation between the spectral bands and the agronomic parameters. For the red region, Pearson correlation coefficients (PCC) were 0.293 (P-value = 0.000); 0.371 (P-value = 0,000), and 0.137 (P-value = 0.039) for height, crown diameter and number of nodes, respectively. However, for the green region, the correlation coefficient for the variable crown diameter was 0.150 (P-value = 0.023). For near-infrared, the correlation coefficients for height, crown diameter and number of nodes were, respectively, 0.407 (P-value = 0.000), 0.389 (P-value = 0.000), and 0.173 (P-value = 0.009).

The April's flight presented significant correlation between the spectral bands and the agronomic parameters. For the red region, the Pearson correlation coefficients (PCC) were 0.433 (P-value = 0.000); 0.470 (P-value = 0.000), and 0.213 (P-value = 0.001) for height, crown diameter, plagiotropic branches length, and number of nodes, respectively. However, for the green region, the correlation coefficient for the variables height, crown diameter, and plagiotropic branches length were, respectively, 0.249 (P-value = 0.000); 0.376 (P-value = 0.000), and 0.143 (P-value = 0.031). For the near-infrared region, the correlation coefficient for height, crown diameter, and number of nodes after the pruning point were, respectively, -0.392 (P-value = 0.000); -0.395 (P-value = 0.000), and -0.258 (P-value = 0.000).

The June's flight presented significant correlation between the spectral bands and the agronomic parameters. For the red region, the Pearson correlation coefficient (PCC) were 0.254 (P-value = 0.000); 0.295 (P-value = 0.000), and 0.134 (P-value = 0.043) for height, crown diameter, and plagiotropic branches length. However, for the green region, the correlation coefficient for the variables height and crown diameter were, respectively, 0.141 (P-value = 0.033), and 0.248 (P-value = 0.000). For near-infrared, the correlation coefficients for height, crown diameter, plagiotropic branches length, number of nodes, and number of plagiotropic branches after the pruning point were, respectively, 0.375 (P-value = 0.000); 0.338 (P-value = 0.000); 0.218 (P-value = 0.001); 0.169 (P-value = 0.011), and 0.188 (P-value = 0.004).

The September's flight presented significant correlation between the spectral bands and the agronomic parameters.

For the red region, Pearson correlation coefficients (PCC) were 0.137 (P-value = 0.038); 0.139 (P-value = 0.036) for height and number of plagiotropic nodes after the pruning point. However, for the green region, the correlation coefficient for the variables height, crown diameter, and the number of plagiotropic branches after the pruning point were, respectively, 0.225 (P-value = 0.001); 0.188 (P-value = 0.004), and 0.173 (P-value = 0.009). For the near-infrared region, the correlation coefficients for height, crown diameter, and number of plagiotropic branches after the pruning point were, respectively, 0.225 (P-value = 0.001); 0.154 (P-value = 0.020), and 0.213 (P-value = 0.001).

Table 1 presents the simple parametric regression models generated based on the significant correlations.

February, April, June, and September's flights presented correlation with many agronomic parameters. Then, the regression models were generated for the estimation of the vegetative characteristic researched. For the parameter height in February, April, and June, the band that presented the most precise model, lower RMSE, was B_{980nm}, with respective percentages of 8.15; 8.13 e 10.02%. In September, B_{560nm} presented the most precise model (RMSE = 12.43%).

Table 1: Linear regressions and RMSE of the significant correlations

Agronomic parameter	Flight date	Band	Regression equation	P-value	RMSE	RMSE (%)
Height	02/13/2020	$B_{650\ nm}$	=1.5421+(0.001586*B1)	0.000	0.154	8.45
		$B_{980\ nm}$	**=0.898+(0.003713*B3)**	**0.000**	**0.149**	**8.15**
	04/20/2020	$B_{650\ nm}$	=1.079+(0.00369*B1)	0.000	0.160	8.34
		$B_{560\ nm}$	=1.587+(0.001769*B2)	0.000	0.167	8.73
		$B_{980\ nm}$	**=2.4304-(0.002924*B3)**	**0.000**	**0.156**	**8.13**
	06/24/2020	$B_{650\ nm}$	=1.433+(0.002658*B1)	0.000	0.209	10.33
		$B_{560\ nm}$	=1.776+(0.001041*B2)	0.033	0.207	10.21
		$B_{980\ nm}$	**=0.868+(0.004713*B3)**	**0.000**	**0.203**	**10.02**
	09/01/2020	$B_{650\ nm}$	=1.838+(0.001636*B1)	0.038	0.263	12.74
		$B_{560\ nm}$	**=1.693+(0.002186*B2)**	**0.001**	**0.256**	**12.43**
		$B_{980\ nm}$	=1.418+(0.002683*B3)	0.001	0.257	12.47
Crown diameter	02/13/2020	**$B_{650\ nm}$**	**=1.2538+(0.00325*B1)**	**0.000**	**0.215**	**11.69**
		$B_{560\ nm}$	=1.59+(0.001287*B2)	0.023	0.227	12.32
		$B_{980\ nm}$	=0.418+(0.005586*B3)	0.000	0.220	11.96
	04/20/2020	**$B_{650\ nm}$**	**=0.814+(0.004471*B1)**	**0.000**	**0.195**	**10.64**
		$B_{560\ nm}$	=1.267+(0.002974*B2)	0.000	0.198	10.80
		$B_{980\ nm}$	=2.392-(0.003194*B3)	0.000	0.196	10.69
	06/24/2020	$B_{650\ nm}$	=1.086+(0.003974*B1)	0.000	0.262	13.61
		$B_{560\ nm}$	**=1.336+(0.002835*B2)**	**0.000**	**0.252**	**13.11**
		$B_{980\ nm}$	=0.646+(0.00534*B3)	0.000	0.257	13.39
	09/01/2020	$B_{560\ nm}$	=1.529+(0.002509*B2)	0.004	0.277	14.54
		$B_{980\ nm}$	**=1.462+(0.002031*B3)**	**0.020**	**0.270**	**14.19**
Plagiotropic branches length	04/20/2020	**$B_{650\ nm}$**	**=1.257+(0.00339*B1)**	**0.001**	**0.357**	**17.78**
		$B_{560\ nm}$	=1.604+(0.00223*B2)	0.031	0.365	18.16
	06/24/2020	$B_{650\ nm}$	=1.67+(0.00177*B1)	0.043	0.442	21.92
		$B_{980\ nm}$	**=1.067+(0.00409*B3)**	**0.001**	**0.434**	**21.56**
Number of nodes	02/13/2020	$B_{650\ nm}$	=64.15+(0.0502*B1)	0.039	14.99	20.77
		$B_{980\ nm}$	**=43.9+(0.117*B3)**	**0.009**	**14.81**	**20.52**
	06/24/2020	**$B_{980\ nm}$**	**=47.9+(0.1466*B3)**	**0.011**	**17.67**	**22.93**
Number of plagiotropic branches from the pruning point	04/20/2020	$B_{650\ nm}$	=-3.58+(0.1393*B1)	0.000	9.422	33.68
		$B_{980\ nm}$	**=49.05-(0.1198*B3)**	**0.000**	**9.402**	**33.61**
	06/24/2020	**$B_{980\ nm}$**	**=9+(0.1294*B3)**	**0.004**	**12.32**	**30.43**
	09/01/2020	$B_{650\ nm}$	=35.18+(0.0602*B1)	0.036	14.83	38.11
		$B_{560\ nm}$	=30.22+(0.0783*B2)	0.009	14.72	37.82
		$B_{980\ nm}$	**=16.1+(0.1139*B3)**	**0.001**	**14.40**	**37.01**

In bold letters are the regressions that presented p-value (<0.05) and low RMSE (%).

The model selected to generate the estimation model was the one that presented the lower RMSE (8.13%) among all models generated, being it the month of April and the band B_{980nm}.

The most precise models for the parameter crown diameter in February and April were related to B_{650nm}, presenting RMSE of 11.69 and 10.64%, respectively (Table 1). In June, the most precise model was B_{560nm} (RMSE = 13.11%), and in September was B_{980nm} (RMSE = 14.19%). Thus, the most precise model to estimate the variable crown diameter was related to April's flight and the band B_{650nm}, presenting an accuracy of 89.36%.

For the length of plagiotropic branches, the most precise model generated for April was with B_{650nm} (RMSE = 17.78%), and, in June, the model generated with B_{980nm} presented RMSE of 21.56%. Therefore, the model selected for the variable estimation was related to April with an accuracy of 82.22%.

The regression models generated for February and June concerning the number of nodes were more precise with B_{980nm}, presenting RMSE = 20.52 and 22.93%, respectively. Thus, the model selected to estimate this variable was related to February with an accuracy of 79.48%.

The parameter number of plagiotropic branches after the pruning point presented the most precise models with B_{980nm} in April, June, and September (RMSE = 33.61, 30.43, 37.01%, respectively). The model selected was related to June's flight presenting an accuracy of 69.57%.

Figure 1 presents the thematic maps generated through the regression model for plants' height developed in April's flight and B_{980nm} (Figure 2A) and the growth rates of February concerning April (Figure 2B), June (Figure 2C), and September (Figure 2D).

The plants' height gradually increased during the months evaluated. The lower RMSE (8.13%) was obtained in April, and the band B_{980nm} (Table 1). It was the most precise model to estimate this parameter, presenting 91.87% precision. Mean growths of 6.9, 3.6, and 4.5 cm per month were observed for February concerning April (Figure 2B), June (Figure 2C), and September (Figure 2D), respectively. As depicted by Figure 2C regarding the growth rate between February and June, the height growth values in most of the experiment were null, a behavior related to the low temperatures in the period between May and June.

For better vegetative development of coffee tree plants, the ideal temperatures are between 24 and 28 ºC as lower

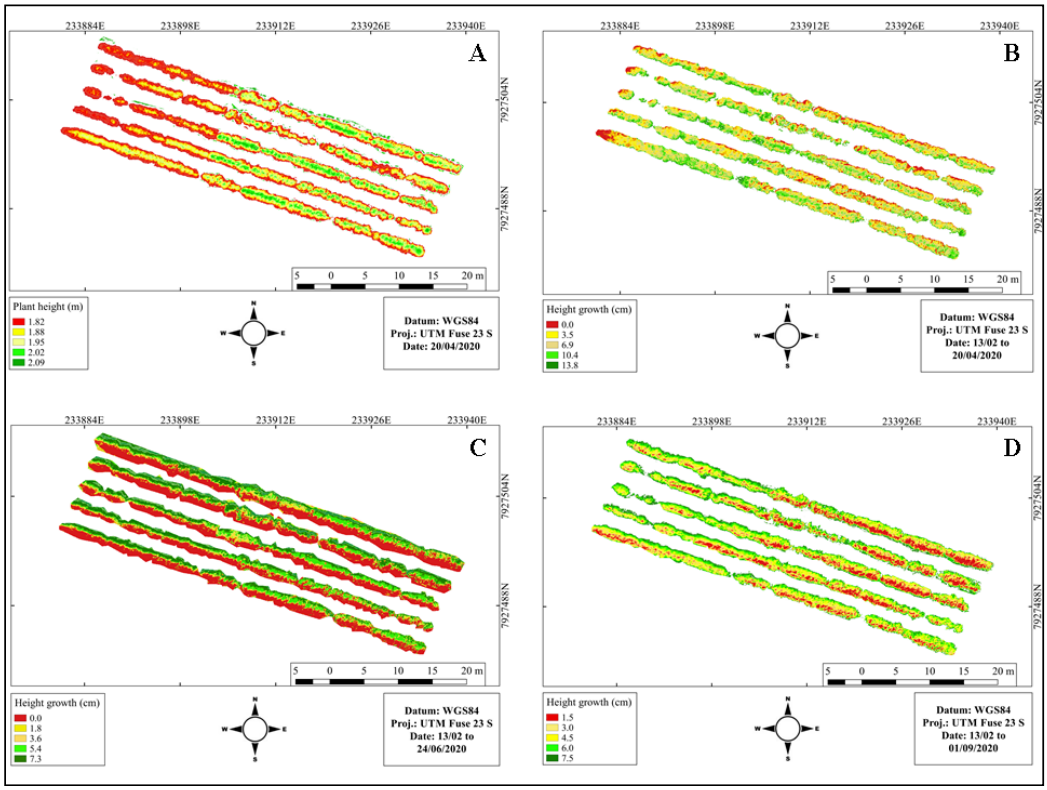

Figure 2: Map of plants' height growth (m) and the April's flight (A); growth rates (cm) of February's flight compared with the flights of April (B), June (C), and September 2020 (D).

temperatures reduce the plants' metabolism (Livramento, 2010). Similar results were found by Partelli *et al*. (2010), who verified a reduction in plagiotropic branch growth rates in coffee trees at temperatures lower than 17ºC. Amaral *et al*. (2009) also verified in coffee plantations that shoot and foliar area's growth rates in all treatments decreased around March, reaching the lower values in May and June due to the low temperatures in the period.

Figure 2 presents the thematic maps generated through the regression model for the variable crown diameter, developed in April's flight and B_{650nm} (Table 1), and the growth rates of February concerning April (Figure 3B), June (Figure 3C), and September (Figure 3D).

The parameter crown diameter increased gradually during the months. The model that presented the lower RMSE (10.64%) was April and the band B_{650nm} (Table 1), which was the most precise to estimate this variable after pruning. Afterward, a thematic map was generated with a precision of 89.26% (Figure 3A). In the growth rates of February concerning April (Figure 3B), June (Figure 3C), and September (Figure 3D), it is observed a mean growth respectively of 7.8, 3.6, and 4.9 cm per month. Due to the low temperatures between May (19ºC) and June (15ºC), the growth rates in February and June (Figure 3C) were null in most of the experiment.

Dubberstein *et al*. (2017) state that seasonal periodicity during coffee tree cycles affects vegetative development, presenting oscillations between increase and stagnation of growth rates. Environmental conditions that influence this development seasonality are climatic variations, either low or high temperatures, rainfall excess, and drought.

Figure 3 presents the thematic maps generated through the regression model for plagiotropic branches length developed in April's flight and the band B_{650nm} (Table 1), and the growth rate between April and June (Figure 4B).

Plagiotropic branch length, as in the parameters presented before, gradually increased during the months. The most precise model to estimate this parameter after pruning was April's flight. The significant correlation with B_{650nm} generated a model with lower RMSE (17,78%) (Table 1), then it was possible to estimate the variable with a precision of 82,22% (Figure 4A). The growth rate between April and June (Figure 4B) presented an average of 2,6 cm per month, and it was null in most of the experiment due to the low temperatures in May and June. It was similar to the behavior observed regarding crown diameter growth rate in the same period.

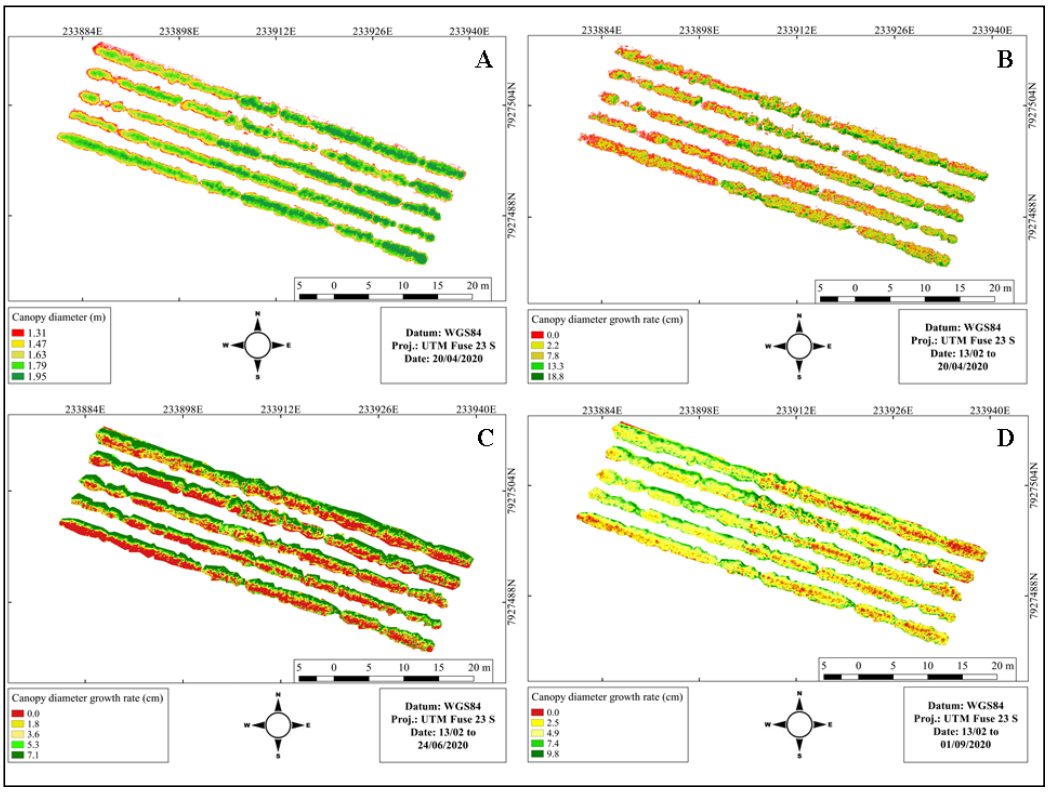

Figure 3: Map of the growth of crown diameter (m) and April's flight (A); growth rate (cm) of February's flight compared with the flights of April (B), June (C), and September 2020 (D).

Cultures' productivity is directly related to phytotechnical growth, vegetative vigor, and plants' biomass accumulation. In this sense, many studies were developed to estimate cultures' productivity, inferring that the more vigorous the plant, the higher its biomass accumulation, then its productivity. Normally, vegetation indices are used to estimate the soil's vegetation cover, phytomass, and photosynthetic activity (Formaggio & Sanches, 2017).

Monitoring parameters such as leaf area index (LAI) in agriculture has been a strategy to identify farms' adversities. The relation between the vegetation's spectral response and the bands obtained through sensors attached to UAVs provides information about plants' phytosanitary conditions. Resende *et al*. (2020) demonstrate radiometric models' potential to estimate LAI, obtained through linear regression models composed by the bands with better correlation with the parameters researched. The results obtained demonstrated the efficiency and higher precision in estimating LAI for the radiometric model composed by a near-infrared band in the camera *MAPPIR 3*.

Figure 4 presents the thematic maps generated through the regression model for the variable number of nodes developed in February's flight and the band B_{980nm} and (Figure 5A), and the growth rates between February and June (Figure 5B). Also, the growth rate of number of plagiotropic branches after the pruning point, developed between April's concerning June (Figure 5C), and September (Figure 5D).

The number of nodes gradually increased during the months. The model that presented the lower RMSE (20.52%) was February and the band B_{980nm} (Table 1), and it permitted to estimate the variable with a precision of 79.48% (Figure 5A) after pruning. February's growth rate compared with June's demonstrated a mean development of 3 nodes per month (Figure 5B). Still, it was null in most of the experiment due to low temperatures between May and June.

The products obtained by multispectral images, either through satellite or UAVs, presented each vegetation's characteristic patterns. Stages of vegetative development – such as the phenological phases of the culture researched, plants' vegetative vigor, space, nutritional and sanitary situation, biotic and abiotic stressors – alter spectral response generating a product (multispectral images) with response patterns between the bands and the variable researched (Barton, 2012).

The research of Almeida *et al*. (2017) estimated the productivity of a coffee farm through agrometeorological modeling and spectral data in *NDVI* of the sensor *MODIS*, generating data with high accuracy with a value of r^2 varying between 0.79 and 0.95, which emphasized this tool's potential in coffee production.

The number of plagiotropic branches after the pruning point is a plant's response to the pruning's handling. Decotetype pruning is characterized by the removal of the superior third of the plants. Through this stimulus, the plant produces new apical buds, which, by their turn, produce new productive or plagiotropic branches (Fernandes *et al*., 2012).

Thus, the number of plagiotropic branches presented a significant correlation with the bands, from April's flight onwards, and the model that generated the lower RMSE (30.43%) (Table 1) was the June's flight with the band 3 (NIR). Therefore, the model estimates the variable with a precision of 69.57% (Table 1). The growth rate related to June (Figure 5C) and September (Figure 5D) presented an average of 5 and 3 plagiotropic branches per month, and due to the lower temperatures in May and June, June presented a null development in most of the experiment.

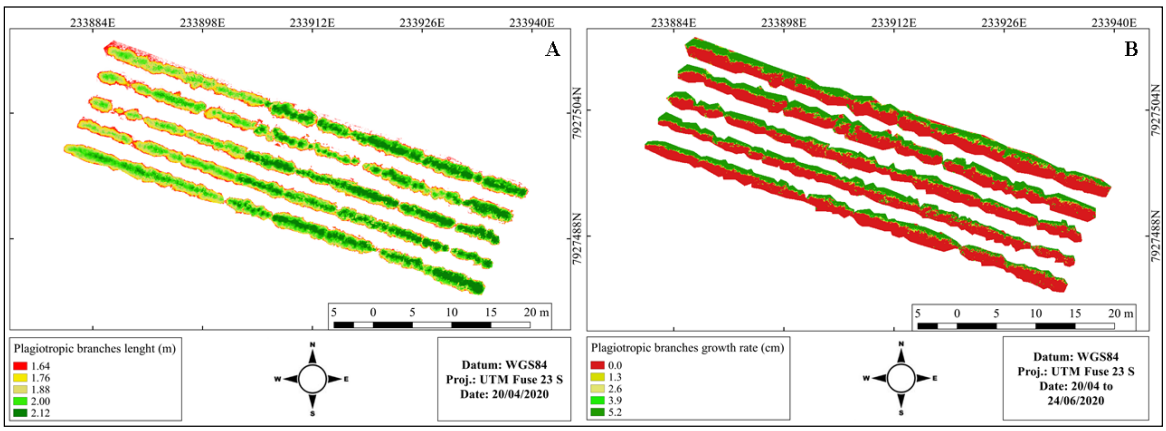

Figure 4: Map of the growth of plagiotropic branches length (m) and April's flight (A); growth rate (cm) of April's flight compared with June's flight (B).

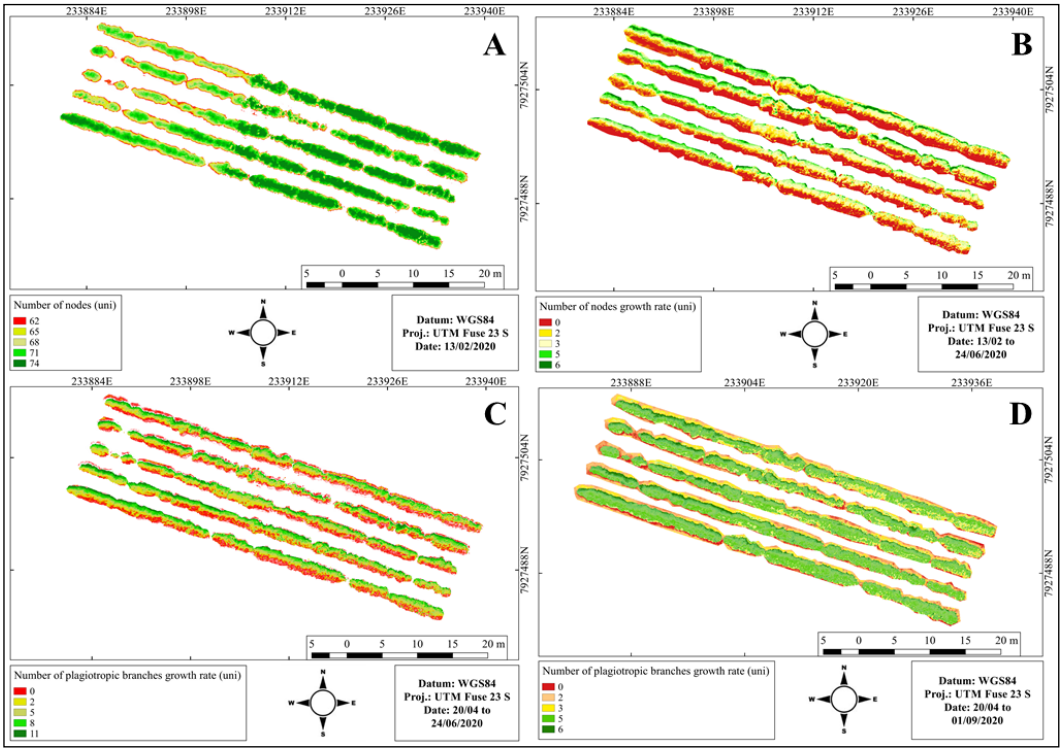

Figure 5: Map of growth in the number of nodes (unit) and February's flight (A); growth rate (unit) of February's flight compared with June's flight (B), growth rate in the number of plagiotropic branches after the pruning point of April's flight compared with June's (C) and September's flight (D).

Santos *et al.* (2019) demonstrate that it is possible to detect symptoms of grey leaf spot in coffee trees using an orthomosaic obtained through multispectral images from a UAV with a spatial resolution of 0.012 m. The vegetation index ExGR satisfactorily segmented the vegetation soil, decreasing at the same proportion of leaf area due to disease infestation or harvest. Marin *et al*. (2019) also demonstrated that vegetation indices presented a distribution similar to the spatial distribution of agronomic variables in the farm, such as coffee leaf miner infestation, silt and clay content in the soil, and concentrations of magnesium, copper, boron, and manganese in the leaves.

Therefore, this research demonstrated the potential of using multispectral images to estimate the phytotechnical development of coffee cultivars after pruning. Thus, the producer may have an estimation tool for vegetative characteristics of different coffee trees' genotypes after pruning and define the most appropriate period to monitor the farm, constituting a basis for future research related to these parameters.

CONCLUSIONS

The use of multispectral images permits the identification of phytotechnical parameters after decote-type pruning and the most appropriate month to estimate each variable.

Based on significant correlations following the Pearson correlation coefficient between the parameters evaluated in February, April, June, and September 2020's flights and the red, green, and near-infrared bands, it was possible to estimate the parameter after decote-type pruning with high accuracy. The height model was estimated through April's flight and the near-infrared band, with 91.87% precision; crown diameter through April's flight and the red band, with 89.36% precision; plagiotropic branches length through April's flight and the red band, with 82.22% precision; the number of nodes through February's flight and the near-infrared band, with 79.48% precision; and the number of plagiotropic branches after the pruning point through June's flight and the near-infrared band, with 69.57% precision.

ACKNOWLEDGEMENTS, FINANCIAL SUPPORT AND FULL DISCLOSURE

To Universidade Federal de Uberlândia (UFU) by the financial support.

Authors declare there is no conflict of interests in carrying the research and publishing this manuscript.

REFERENCES

Almeida TS, Sediyama GC & Alencar LP (2017) Estimativa da produtividade de cafeeiros irrigados pelo método zona agroecológica espectral. Revista Engenharia na Agricultura, 25:01-11.

Amaral JAT, Rena AB & Amaral JFT (2009) Crescimento vegetativo sazonal do cafeeiro e sua relação com fotoperíodo, frutificação, resistência estomática e fotossíntese. Pesquisa Agropecuária Brasileira, 41:377-384.

Assis GA, Silva LRS, Martins WER, Carvalho FJ & Pires PS (2018) Crescimento e produtividade de cafeeiros na região do Alto Paranaíba em função do tipo de poda de desbrota. Revista Ci*ê*ncia Agr*ícola*, 16:09-12.

Barton CVM (2012) Advances in remote sensing of plant stress. Plant and Soil, 354:41-44.

Dubberstein D, Partelli FL, Dias JRM & Espindula MC (2017) Influência da adubação no crescimento vegetativo de cafeeiros na Amazônia Sul Ocidental. Coffee Science, 12:197-206.

Fernandes ALT, Santinato F, Santinato R & Michelin V (2012) Condução das podas do cafeeiro irrigado por gotejamento cultivado no cerrado de Minas Gerais. Enciclopédia Biosfera, 8:487-494.

Formaggio AR & Sanches ID (2017) Sensoriamento remoto em agricultura. São Paulo, Oficina de Textos. 288p.

Freitas RASM, Martins GD, Assis GA, Siquieroli ACS, Fernandes MIS, Soares MOQS & Pinheiro BECCS (2023) Hyperspectral characterization and estimation models for agronomic parameters of coffee cultivars after pruning. Precision Agriculture, 24:2374-2394.

Livramento DE (2010) Morfologia e fisiologia do cafeeiro. In: Reis PR & Cunha RL (Eds.) Café arábica: do plantio à colheita. Lavras, Epamig. p.87-162.

Mahajan GR, Sahoo RN, Pandey RN, Gupta VK & Kumar D (2014) Using hyperspectral remote sensing techniques to monitor nitrogen, phosphorus, sulphur and potassium in wheat (*Triticum aestivum* L.). Precision Agriculture, 15:499-522.

Marin BD, Alves MC, Pozza EA, Gandia RM, Cortez ML & Mattioli MC (2019) Sensoriamento remoto multiespectral na identificação e mapeamento das variáveis bióticas e abióticas do cafeeiro. Revista Ceres, 66:142-153.

Partelli FL, Vieira HD, Silva MG & Ramalho JC (2010) Crescimento vegetativo sazonal em ramos de diferentes idades do cafeeiro conilon. Semina: Ciências Agrárias, 31:619-626.

Resende DB, Abreu-Júnior CAM, Martins GD, Marques OJ & Xavier LCM (2020) Uso de imagens tomadas por aeronaves remotamente pilotadas para detecção da cultura do milho infestada por *Spodoptera frugiperda*. Revista Brasileira de Geografia Física, 13:156-166.

Santos AF, Silva RP, Zerbato C, Menezes PC, Kazama EH, Paixão CSS & Voltarelli MA (2019) Use of real-time extend GNSS for planting and inverting peanuts. Precision Agriculture, 20:840-856.